Electronic and optical properties of CdS/CdZnS nanocrystals*

A. John Peter[a)b)†] and Chang Woo Lee[a)]

[a)] *Department of Chemical Engineering and Green Energy Center, College of Engineering, Kyung Hee University, 1 Seochun, Gihung, Yongin, Gyeonggi 446-701, S. Korea*

[b)] *Department of Physics, Govt. Arts College, Melur, Madurai-62510, India*

(Received 17 November 2011; revised manuscript received 8 April 2012)

$Cd_{1-x}Zn_xS$ nanocrystals are prepared by a co-precipitation method with different atomic fractions of Zn. The texture, structural transformation and optical properties with increasing x value in $Cd_{1-x}Zn_xS$ are studied with scanning electron microscopy, electron diffraction patterning, and absorption spectra respectively. Quantum confinement in a strained $CdS/Cd_{1-x}Zn_xS$ related nanodot with various Zn content values is investigated theoretically. Binding energies on exciton bound $CdS/Cd_xZn_{1-x}S$ quantum dot are computed, with consideration of the internal electric field induced by the spontaneous and piezoelectric polarizations, and thereby the interband emission energy is calculated as a function of the dot radius. The optical band gap from the UV absorption spectrum is compared with the interband emission energy computed theoretically. Our results show that the average diameter of composite nanoparticles ranges from 3 nm to 6 nm. The X-ray diffraction pattern shows that all the peaks shift towards the higher diffracting angles with an increase in Zn content. The lattice constant gradually decreases as the Zn content increases. The strong absorption edge shifts towards the lower wavelength region and hence the band gap of the films increases as the Zn content increases. The values of the absorption edge are found to shift towards the shorter wave length region and hence the direct band gap energy varies from 2.5 eV for the CdS film and 3.5 eV for the ZnS film. Our numerical results are in good agreement with the experimental results.

Keywords: quantum dots, quasicrystals, semiconductor

PACS: 73.21.Fg, 71.55.–i **DOI:** 10.1088/1674-1056/21/8/087302

1. Introduction

II–VI semiconducting materials have emerged with high potential in applications for fabricating optical devices which include short wavelength emitting laser diodes and light emitting diodes operating in the blue region due to their wide direct band gap properties. It is a subject of great interest in regard to chalcogenide-based semiconducting materials which are used in making devices like photodetectors and photovoltaic devices. For example, Cadmium zinc sulfide (CdZnS) ternary compounds are widely used as wide band gap window materials in heterojunction solar cells and photoconductive devices. In solar cell systems, CdS films have been demonstrated to effectively replace CdS with the higher band gap ternary material such as a CdZnS compound which leads to a decrease in window absorption loss. Eventually, an increase in the short-circuit current in the solar cell occurs.[1] Thus CdZnS ternary compounds are potentially useful as window materials for the fabrication of pn junctions without the lattice mismatch in the devices based on quaternary materials like $CuIn_xGa_{1-x}Se_2$[2] or $CuIn(S_zSe_{1-z})_2$.[3]

The exciton energy levels and the optical transitions of CdTe quantum dots have been evaluated using the exact diagonalization by Manaselyan and Chakraborty.[4] There are numerous reports on the optical properties of various metals and rare earth ions doped ZnS, CdS, ZnSe, and CdSe nanostructures, but studies on their doped alloy nanostructures are still limited.[5–8] Doping different activator ions (acting as recombination centres) in these stabilized nanostructures not only gives the chance to obtain the required emission colour, but also to reduce the self-quenching by intrinsic defects in the nanocrystals.[9] In this case it is possible to adjust the lattice matching as well as the electron affinity of the layers with one of the p-type semiconducting substrates by appropriately choosing the solid solution composition. The band gap of ZnCdS can be tuned, depending on the alteration of the content of its constituent.[10] ZnCdS

†Corresponding author. E-mail: a.john.peter@gmail.com

© 2012 Chinese Physical Society and IOP Publishing Ltd

is widely used as a wide-band-gap window material in heterojunction solar cells,[11] low-voltage cathode luminescence,[8] high-density optical recording, and blue and ultraviolet laser diodes.[12]

II–VI compound semiconducting nanocrystals have attracted much attention, owing to their unique optical properties that can be tuned not only by changing the particle size but also by changing the composition of the alloy.[13−15] Among them, the wide band gap nanocrystalline materials have opened a new avenue to tremendous potential applications in diverse areas like solar cells, photo-catalysis, sensors, photonic, and other optoelectronic devices.[16−19] Considerable efforts have been devoted to high temperature synthesis of $Cd_{1-x}Zn_xS$ ($0 \leq x \leq 1$) nanocrystalline thin films by chemical vapour deposition (CVD), molecular beam epitaxy (MBE), metal organic vapour phase epitaxy (MOVPE), and the RF-sputtering method,[20−22] but much less attention is paid to the low temperature chemical synthesis of high-quality water soluble alloy nanocrystals. Nanocrystals synthesized by chemical route give a chance to control their sizes and distribution. One must change the concentration of the reagents and their mixing rates at different temperatures in order to improve the crystallinity.[23] These small-size nanostructures have a large surface-to-volume ratio and they play a dominant role in optical properties of the nanostructures. Various kinds of capping agents and inorganic shells are used to passivate the undesired sites resulting in the enhancement of luminescence intensity to produce good quality nanomaterials.[24]

In the present study, the electrical and optical properties of the influence of Zn substitution in CdZnS material are investigated. We synthesize the $Cd_{1-x}Zn_xS$ ($x = 0 \sim 1$) alloy nanocrystals by the chemical route method and determine their optical band gaps from the absorption spectra. Simultaneously, the effect of optical properties on the theoretical computation is investigated by considering the synthesized nanopowders as quantum dots. We use the variational technique within a single band effective mass approximation to calculate the binding energy and the optical band gap. In Section 2, we present the method (experimental and theoretical techniques) following our model while the results and discussion are presented in Section 3. Conclusions are summarized in Section 4.

2. Model and calculations

2.1. Experiment

The following procedure was carried out to prepare the CdZnS nanocrystals. For the dopant source, zinc chloride was used for the dopant Zn source and cadmium chloride served as dopant for the cadmium source. A solution of 0.02-M cadmium chloride and 0.15-M thiourea were mixed and precipitated with sodium hydroxide (0.4 M) under vigorous stirring at 60 °C for 1 h. The resulting solution was stirred for 1 h and then the $ZnCl_2$ solution with an appropriate ratio was added into it. The precipitated pale yellow colloidal solution was obtained at the end. The formed nanopowders were separated from the reaction medium by centrifugation. They were washed with de-ionised water and ethanol to remove the impurities and then dried at 80 °C. To investigate the structural and optical properties, the samples were characterized by X-ray diffraction on a Philips X'pert–MPD X-ray diffractometer with Cu Ka. The UV–Vis absorption spectra were measured on a Hitachi model U-3300 spectrophotometer.

2.2. Theory

Within the framework of single band effective mass approximation, the Hamiltonian of the exciton considering a strained $CdS/Cd_xZn_{1-x}S$ quantum dot with radius R, can be written as

$$\left[-\frac{\hbar^2}{2m^*_{\mathrm{e,h}}}\frac{1}{r_{\mathrm{e,h}}}\frac{\partial^2}{\partial r^2_{\mathrm{e,h}}}r^2_{\mathrm{e,h}} + V_{\mathrm{e,h}}(r_{\mathrm{e,h}}) + \frac{P_Z^2}{2M} + \frac{p_z^2}{2\mu} - \frac{e^2}{\varepsilon\,|r_{\mathrm{e}} - r_{\mathrm{h}}|} - E\right]\psi_{\mathrm{e,h}}(r_{\mathrm{e,h}}) = 0, \quad (1)$$

where $m^*_{\mathrm{e,h}}$ are the effective masses of electron and hole, ε is the dielectric constant for the material inside the quantum dot, $|\bar{r}_{\mathrm{e}} - \bar{r}_{\mathrm{h}}|$ denotes the relative distance between the electron and the hole, and $V_{\mathrm{e,h}}$ is the confined potential of conduction band and valence band. The band gap of the material is given by

$$E_{\mathrm{g}}(Cd_xZn_{1-x}S) = 2.566 + 0.041x + 1.086x^2 \ (\mathrm{eV}). \quad (2)$$

The above expression of band gap has been obtained by varying the Cd concentration in ZnS powders (Fig. 1) through taking various concentrations of Cd and thereby calculating the optical energy band gap. Similar expressions have been obtained in Refs. [25] and [26]. The quadratic term in Eq. (2) is correlated

with the bowing of the optical band gap.[27] This approximation directs us to distribute the band gap discontinuities between $Cd_xZn_{1-x}S$ dot and ZnS barrier as $V(z) = 0.7\Delta E_g$.

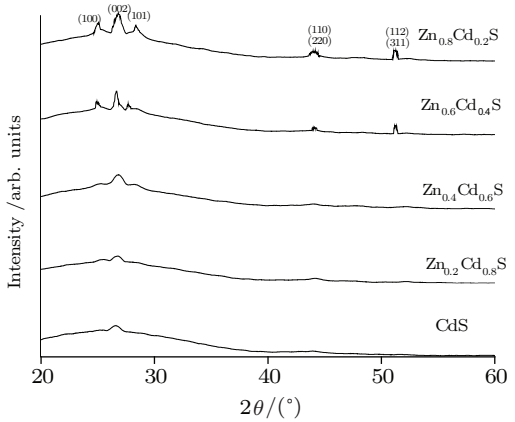


Fig. 1. X-ray diffraction patterns for $Zn_xCd_{1-x}S$ powders with different Zn content values.

The strain-induced potential for the conduction band can be expressed as[28]

$$V_{\text{Cstrian}} = a_c(\varepsilon_{xx} + \varepsilon_{yy} + \varepsilon_{zz}), \tag{3}$$

where a_c is the deformation potential constant of the conduction band, $\varepsilon_{xx} = \varepsilon_{yy} = (a_0 - a)/a$ with a_0 being the equilibrium lattice constant for the strained layer and a the unstrained lattice constant and $\varepsilon_{zz} = -2(C_{12}/C_{11})\varepsilon_{xx}$, the values of the parameters are given in Table 1. Semiconductor alloys have been proposed to obey Vegard's law, revealing the linear relationship between the lattice constants and composition as given by[29]

$$a^0_{Cd_{1-x}Zn_xS}(x) = xa^0_{ZnS} + (1-x)a^0_{CdS}. \tag{4}$$

Table 1. Material parameters used in the calculations (linearly interpolated from the data of ZnS and CdS) used in the calculations.

Parameter	CdS	$Cd_{0.6}Zn_{0.4}S$	$Cd_{0.4}Zn_{0.6}S$	ZnS
m^*_e	0.21	0.267	0.343	0.40
γ_1	3.158	3.027	2.852	2.721
γ_2	0.746	0.774	0.812	0.841
ε_{31}	–0.159	–0.159	–0.16	–0.16
ε_{33}	0.347	0.306	0.251	0.21
C_{13}/GPa	39.4	49.96	64.04	74.6
$C33$/GPa	93.8	90.17	85.33	81.7
ε	8.9	8.78	8.62	8.5
a_c/eV	–0.24	1.395	2.935	4.09 eV
a_v/eV	0.56	1.08	1.785	2.31 eV
a/nm	0.582	0.57	0.553	0.541

The strain-induced potential for the valence band can then be written as[30]

$$V_{\text{Vstrain}} = a_v(\varepsilon_{xx}+\varepsilon_{yy}+\varepsilon_{zz}) - \frac{b}{2}(\varepsilon_{xx}+\varepsilon_{yy}-2\varepsilon_{zz}), \tag{5}$$

where a_v and b are the deformation potential constants of the valence band.

The strength of the built-in electric field F caused by the spontaneous and piezoelectric polarizations in the $CdS/Zn_xCd_{1-x}S$ strained quantum dot is expressed as[31]

$$F = \begin{cases} \left| -\dfrac{P^{\text{CdS}}_{\text{SP}} + P^{\text{CdS}}_{\text{PE}} - P^{\text{Zn}_x\text{Cd}_{1-x}\text{S}}_{\text{SP}}}{\varepsilon_0 \varepsilon^{\text{CdS}}_e} \right|, & r < R, \\ 0, & r \geq R. \end{cases} \tag{6}$$

Here, $\varepsilon^{\text{CdS}}_e$ is the electronic dielectric constant of CdS and $P^{\text{CdS}}_{\text{PE}}$, $P^{\text{CdS}}_{\text{SP}}$, and $P^{\text{Zn}_s\text{Cd}_{1-x}\text{S}}_{\text{SP}}$ are the piezoelectric polarizations and spontaneous polarizations of CdS and the spontaneous polarization of $Zn_xCd_{1-x}S$, respectively. The above values can be generally calculated by the polarity of the crystal and the strains of the quantum nanostructure. Since the wurtzite crystal lattices of CdS and ZnS lack inversion symmetry, the heterostructure will have spontaneous polarization (P^{SP}) and the piezo electric polarization (P^{PZ}) due to the strain caused by the lattice mismatch between CdS and ZnS material.

The piezoelectric polarization along the c axis is given by

$$P^{\text{PZ}} = e_{31}(\varepsilon_{xx} + \varepsilon_{yy}) + e_{33}\varepsilon_{zz} \tag{7}$$

with

$$\varepsilon_{xx} = \varepsilon_{yy} = \frac{a(\text{CdS}) - a(\text{ZnCdS})}{a(\text{CdS})}$$

and $\varepsilon_{zz} = -2(C_{13}/C_{33})\varepsilon_{xx}$, the values of parameters are given in Table 1. The piezoelectric polarization is given by

$$P^{\text{PZ}} = 2\varepsilon_{xx}\left(e_{31} - \varepsilon_{33}\frac{C_{13}}{C_{33}}\right). \tag{8}$$

Thus the total polarization is given by

$$\boldsymbol{P} = \boldsymbol{P}^{\text{PZ}} + \boldsymbol{P}^{\text{SP}}. \tag{9}$$

Electron (hole) effective mass m^*_j is given by

$$m^*_j = \begin{cases} m^*_{\text{I}}, & r < R, \\ m^*_{\text{II}}, & r \geq R, \end{cases} \tag{10}$$

where m^*_{I} and m^*_{II} denote the reduced effective masses inside and outside the quantum dot. The material parameters are given in Tables 1 and 2.

Table 2. Electron band parameters.*

x	$m_{\rm e}^*$ (m_0)	$m_{\rm hh}^*$ (m_0)	$V_{\rm e}$/meV	$V_{\rm h}$/meV	$E_{\rm g}$/eV
0	0.21	5.00	1796	769	3.53
0.2	0.216	4.352	1832	785	3.24
0.4	0.232	3.704	1929	826	2.99
0.6	0.248	3.056	2087	894	2.78
0.8	0.264	2.408	2305	897	2.62
1.0	0.28	1.76	2584	1108	2.50

*Parameters cited from Refs. [42]–[44].

The reduced mass corresponding to the heavy hole band in the plane perpendicular to the z axis is expressed as

$$\frac{1}{\mu} = \frac{1}{m_j^*} + \frac{1}{m_0}(\gamma_1 + \gamma_2), \tag{11}$$

where m_0 is the free electron mass.

We choose a trial wave function as follows:

$$\Psi(r_{\rm e}, r_{\rm h}) = |\,\psi(r_{\rm e})\rangle\;|\,\psi(r_{\rm h})\rangle\;\psi(z)\rangle\;. \tag{12}$$

The ground state wave function of the electron (hole) confined in the strained CdS/$Cd_xZn_{1-x}S$ quantum dot can be written as

$$\psi(r_j) = \frac{1}{r_j}\varphi(r_j)\mathrm{Y}_l^m(\theta,\phi), \tag{13}$$

where $\mathrm{Y}_l^m(\theta,\phi)$ are the complex spherical harmonics and $\varphi(r)$ is the radial wave function and the corresponding confinement energy equation of the electron (hole) can be obtained by using the m-order Bessel function J_m and the modified Bessel function K_m as

$$\psi(r,\theta,\varphi) = \begin{cases} N_1\,\mathrm{e}^{\pm \mathrm{i}l\phi}\mathrm{J}_l(r_{nl}r), & r < R, \\ N_1\dfrac{\mathrm{J}_l(r_{nl}R)}{\mathrm{K}_l(b_{nl}R)}\,\mathrm{e}^{\pm \mathrm{i}l\phi}\mathrm{K}_l(b_{nl}r), & r \geq R, \end{cases} \tag{14}$$

where N_1 is the normalization constant,

$$r_{nl} = \sqrt{\frac{2m_j^* E_{nlk}}{\hbar^2}}, \tag{15}$$

and

$$b_{nl} = \sqrt{\frac{2m_j^*(V - E_{nlk})}{\hbar^2}}, \tag{16}$$

with r_{nl} being the n-th root satisfying the equation

$$r_{nl}\left.\frac{\mathrm{d}\mathrm{J}_l(r_{nl}r)}{\mathrm{d}(r_{nl}r)}\right|_{r=R} = b_{nl}\left.\frac{\mathrm{J}_l(r_{nl}r)}{\mathrm{K}_l(b_{nl}r)}\frac{\mathrm{d}\mathrm{K}_l(b_{nl}r)}{\mathrm{d}(b_{nl}r)}\right|_{r=R}, \tag{17}$$

and E_{nlk} the lowest binding energy calculated by solving the transcendental equation

$$\sqrt{E}\mathrm{J}_1(\sqrt{E}R)\mathrm{K}_0(\sqrt{(V-E)}R) = (\sqrt{(V-E)}\mathrm{K}_1(\sqrt{(V-E)}R)\mathrm{J}_0(\sqrt{E}R). \tag{18}$$

This fixes the values of r_{nl} and b_{nl} for the lowest values of E_{nlk} after matching the wave functions and their derivatives at the boundaries of the quantum dot along with the normalization.

The trial wave function $|\,\psi(z)\rangle$ describing the internal motion between the electron and the hole in the system, taken to be the lowest state of the exciton energy, is given by

$$|\,\psi(z)\rangle = \exp(-\alpha_2\rho^2 - \beta_2 z^2), \tag{19}$$

where α_2 and β_2 are the variational parameters. The anisotropic two-parameters, relative to the trial wavefunction, describe the internal motion between the electron and the hole in the complex system. We calculate the ground state energy $E_{\rm exc}$, by finding out the expectation value of the energy of the Hamiltonian, Eq. (1), as

$$\langle E_{\rm exc}\rangle = \min_{\alpha,\beta}\frac{\langle\psi_{r_{\rm e}}\,|H_{\rm exc}|\,\psi_{r_{\rm h}}\rangle}{\langle\psi_{r_{\rm e}}\,|\psi_{r_{\rm h}}\rangle}. \tag{20}$$

The donor exciton binding energy $E_{\rm b}$ and the interband emission energy $E_{\rm ph}$ associated with the exciton are calculated using the following equation:

$$E_{\rm b} = E_{\rm e} + E_{\rm h} - E_{\rm exc}, \tag{21}$$

$$E_{\rm ph} = E_{\rm e} + E_{\rm h} + E_{\rm g} - E_{\rm exc}, \tag{22}$$

where $E_{\rm e}$ and $E_{\rm h}$ are the confinement energies of the electron and hole respectively, and $E_{\rm g}$ is the band gap energy of CdZnS material.

3. Results and discussion

$Cd_{1-x}Zn_xS$ ($x = 0 \sim 1$) nanocrystals are synthesized by the chemical route method for different Zn concentrations, and the absorption spectra are taken to calculate the band gap of the material. Numerical calculations are carried out to compute the donor exciton binding energy in the CdS doped with $Cd_{1-x}Zn_xS$ quantum dot with the heavy hole mass as the heavy excitons are more common in experimental results. The exciton binding energy values and thereby the interband emission energies are computed, each as a function of dot radius for different Zn content values

of the host material. The obtained optical band gaps from the absorption spectra are compared with the interband emission energies obtained by theoretical calculations using the variational technique.

3.1. Structural studies

The structures of $Cd_{1-x}Zn_xS$ nanoparticles, for various Zn content values, are shown in X-ray diffraction patterns in Fig. 1. The figure depicts the $Cd_{1-x}Zn_xS$ nanocrystallites for different values of $x =$ 0.0, 0.2, 0.4, 0.6, and 0.8. The diffraction spectra are obtained by scanning 2θ in a range of 20°–60° and CdS film shows a single diffraction peak at $2\theta = 26.59°$. This peak could be associated with the (002) reflection of the hexagonal modification or the (111) reflection of the cubic modification. It shows the dominant orientation. With a further increase in Zn concentration, the structure exhibits a mixture of both cubic and hexagonal phases as investigated earlier in Refs. [32]–[34] with additional two dominant orientations (101) and (100). It is also noticed that the diffraction peak shifts toward the higher angles when the Zn concentration increases. XRD pattern displays that the well-defined peaks shifting in position and the intensity with change in composition match with JCPDS Card: 40-0834 and 40-0835. The peaks become sharper as the Zn content increases, shifting towards ZnS side. Moreover we observe a gradual decrease in lattice parameters as the Zn content increases. This trend is consistent with Vegard's law, indicating a homogenous alloy structure.[35]

3.2. Morphological studies

Figure 2 shows the field-emission scanning electron microscopy (EF-SEM) images of the surface of ZnS films doped with Zn content values of 0.2, 0.4 0.6, and 0.8 at% on the glass plate separately. They are used to determine the grain sizes of $Cd_{1-x}Zn_xS$ nanopowders, as seen from the SEM images, the particles are well dispersed and their shapes and sizes are clear. SEM is used to determine the grain sizes of $Cd_{1-x}Zn_xS$ powders with a uniform deposition of CdS film which shows texture shape with holes.[36] Texture shapes with holes are depicted in the uniform deposition of films, however, it is observed that the grain sizes in the films increase as the Zn content shifts toward the higher band gap.

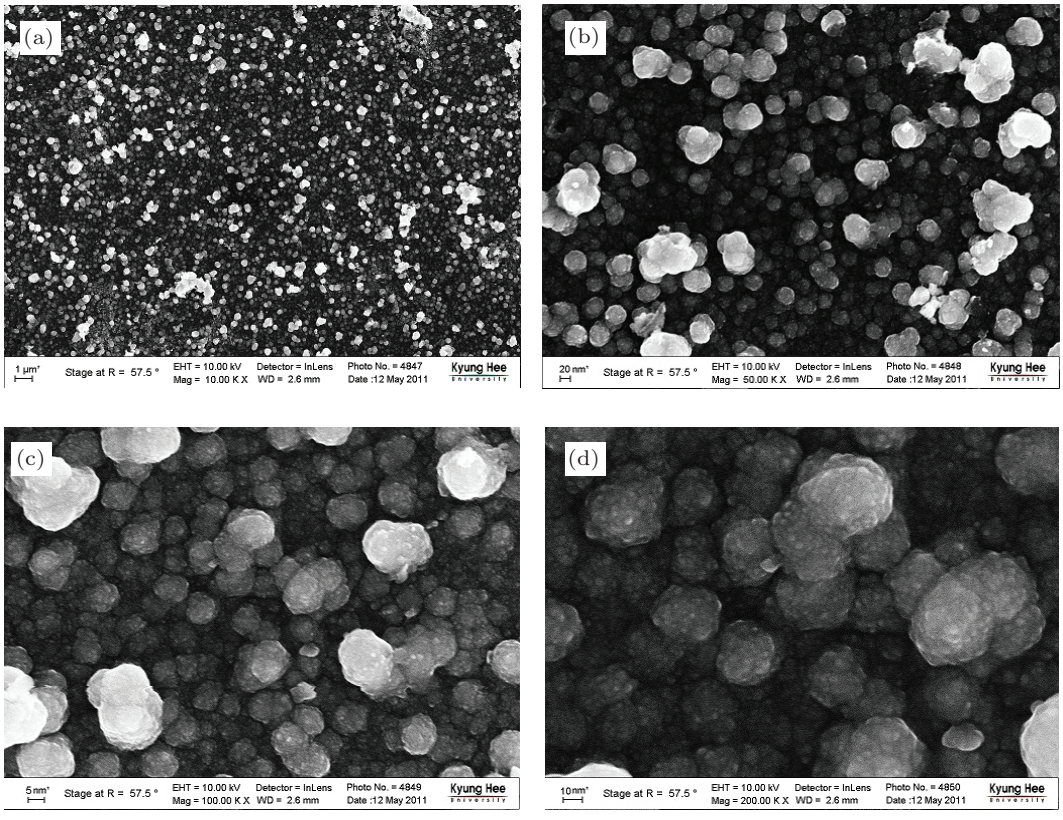


Fig. 2. E-F SEM images of ZnS doped with Cd content values of 0.2, 0.4 0.6, and 0.8 at%, showing SEM micrographs of $Cd_{0.8}Zn_{0.2}S$ (a), $Cd_{0.6}Zn_{0.4}S$ (b), $Cd_{0.4}Zn_{0.6}S$ (c), and $Cd_{0.2}Zn_{0.8}S$ (d).

3.3. Optical studies

Variations of band gap with Cd and Zn concentration increasing are shown in Fig. 3 and the insert shows the variation of barrier height as a function of Cd content. The variation of the composition x of the QD material modifies the energy gap. We observe that the band gap decreases as the Cd content increases and it can be estimated by the expression $E_{\rm g}({\rm Cd}_{1-x}{\rm Zn}_x{\rm S}) = 2.566 + 0.041x + 1.086x^2$ (eV). Moreover, it is noticed that the barrier height of the finite quantum dot increases as the Cd content increases as shown in the insert of the figure. The effect of z-confinement is calculated through a finite quantum dot model with a confinement potential determined by the band offsets and strain effects. The conduction band offset and the valence band offset are obtained to be 1873 meV and 802 meV respectively for $x = 0.3$. These values are obtained by the linear interpolation from the data available for CdS and ZnS materials.

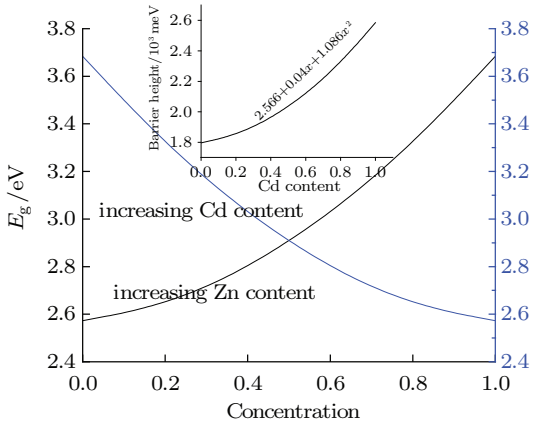


Fig. 3. Variations of band gap with Cd and Zn concentration increasing, with the insert showing the variation of barrier height as a function of Cd content.

Figure 4 shows the plots of $(\alpha h\nu)^2$ versus $h\nu$ of ZnCdS nanopowders with various concentrations of Cd and Zn; and the insert shows the band gap varying with Cd content for the synthesized CdZnS nanocrystals. The absorption spectra of the films are measured to investigate their band gaps for two different Cd concentrations in CdZnS samples. The direct allowed optical band gap $E_{\rm g}$ is estimated from the plots of $(\alpha\lambda v)^2$ versus (λv). As shown in the figure, the absorption spectrum of the CdS film shows a sharp edge in a wavelength range of 350 nm–450 nm. The absorption spectra of the CdZnS films are found to depend on the Cd concentration in solution of the visible region. It is observed that the absorption spectra shift towards longer wavelengths as the concentration of Cd increases. The absorption band edges are localized at 383 nm, 415 nm, 447 nm, and 475 nm for ZnS doped with Cd for 0.2, 0.4, 0.6, and 0.8 at% concentration and the corresponding particles with diameters of 3.2 nm, 4.5 nm, 4.8 nm, and 5.3 nm, respectively. The absorption edges for these nanocrystals show blue-shifts of 20 nm–120 nm by comparing with the absorption edge of the bulk CdS (around 500 nm). The observed band gaps for various Cd content values in ZnS are shown in Table 2 along with the mass parameters for electron and heavy hole with the barrier height. The energy gap values agree with the experimental results in Ref. [38]. Hence it is obvious that as Zn content increases particle size decreases, resulting in a higher band gap due to the increasing contribution of quantum size effect.

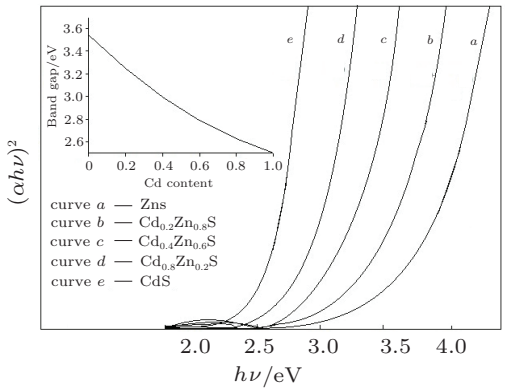


Fig. 4. Plots for α^2 versus $h\nu$ of ZnCdS nanocrystals with various concentrations of Cd, with the insert showing the variation of the band gap with the concentration of Cd.

Variations of exciton binding energy each as a function of dot radius of different concentrations are shown in Fig. 5 and the insert shows the variations of binding energy with Cd content for three different dot radii. In all cases, the exciton binding energy increases as the dot radius decreases, reaching a maximum value and then decreasing when the dot radius is still decreasing. The Coulomb interaction between the electron and hole increases, which ultimately causes the decrease in binding energy when the dot radius decreases. As the dot radius approaches to zero the confinement becomes negligibly small, and in the finite barrier problem the tunnelling becomes huge. From the insert, we find that the binding energy increases with the Cd content increasing. Further, we find that

the exciton binding energy is higher when the dot radius becomes smaller due to the geometrical confinement.

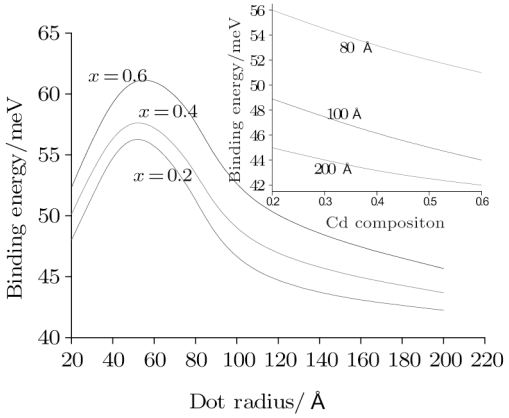


Fig. 5. Variations of exciton binding energy each as a function of dot radius of three different concentrations with the insert showing the variations of binding energy with Cd content for three different dot radii.

In Fig. 6, we present the variations of the optical band gap each as a function of dot radius of CdS/ $Cd_{1-x}Zn_xS$ quantum dot with different content values of Cd. Shadows in the figure refer to the optical band gap values of 30 Å (1 Å = 0.1 nm) and 40 Å quantum dot radius of $Cd_{1-x}Zn_xS$. It is noted that the interband emission energy decreases monotonically as the dot radius increases. This is due to the confinement of the electron–hole with respect to the z-plane when the dot radius increases. Also it is observed that as the concentration of Cd increases the optical band gap decreases due to the reduction of the barrier height. Moreover it is clearly shown that the effect of donor bound exciton

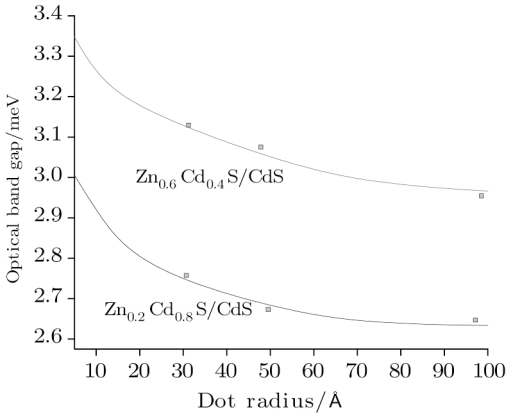


Fig. 6. Variations of the optical band gap each as a function of the dot radius of the $Cd_{1-x}Zn_xS$/CdS quantum dot with different content values of Cd. The squares refer to the experimental data of synthesized material of ZnCdS nanocrystals.

has an influence on the interband emission energy. This representation clearly brings out the quantum size effect. Moreover we observe that the band gap does not vary beyond 60 Å. This result fits closely with the previous investigation.[37]

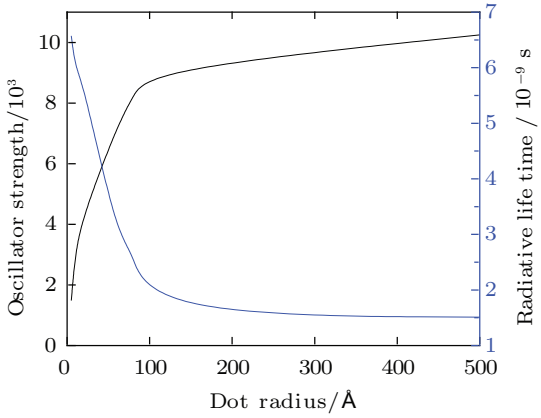


Fig. 7. Varitions of exciton oscillator strength and the radiative life time of the confined exciton with dot radius.

We display the exciton oscillator strength and the radiative life time of confined exciton each as a function of dot radius for $Cd_{0.3}Zn_{0.7}S$ in Fig. 7. In absorption spectra, the intensity of an exciton binding energy and the envelope wave function are characterized by the oscillator strength[38]

$$f = \frac{E_{\rm p}}{E_{\rm exc}} \left| \int_V \psi_{\rm exc}(r)\,{\rm d}r \right|^2 , \tag{23}$$

where the Kane energy of GaN is $E_{\rm p} = 10$ meV. It is observed that the oscillator strength increases with an increase in the dot radius. The radiative life time can be calculated as[39]

$$\tau = \frac{2\pi\varepsilon_0 m_0 c^3 h^2}{\sqrt{\varepsilon} e^2 E_{\rm exc}^2 f}, \tag{24}$$

where f is the oscillator strength, $E_{\rm exc}$ is the exciton binding energy and all the other parameters are universal physical constants. It is found that the radiative life time of exciton decreases as the dot radius increases. The values of radiative life time are almost constant beyond a dot radius of 100 Å. The results fit well with the recent investigations reported by Mohanta *et al.*,[40] who have calculated the radiative life time of $Cd_{0.25}Zn_{0.75}S$ nanocrystals to be 1.64 ns. Moreover, Wang *et al.*,[41] have also reported on the same values.

4. Conclusions

In this paper, we calculated the exciton binding energies and the interband emission energies in the strained CdS/$Cd_xZn_{1-x}S$ quantum dot for different values of x. We considered the effects of geometrical confinement on the optical properties of grown quantum dots of different sizes with the inclusion of a built-in electrostatic field. The theoretical computation is carried out using the variational technique within the single band effective mass approximation. The composite nanoparticles are obtained using the chemical route method with ZnCdS particle diameters ranging from 3 nm to 6 nm. Numerical calculations on the geometrical effects of the optical properties of $Cd_{1-x}Zn_xS$ quantum dots are discussed theoretically. The values of the absorption edge are found to shift towards the shorter wave length region and hence the direct band gap energy varies from 2.5 eV for CdS to 3.5 eV for ZnS powders. Moreover, it is clearly shown that the grain size increases with an increase in Cd concentration in the film. The absorption spectra of the synthesized $Cd_{1-x}Zn_xS$ reveals that their optical band gaps are in good agreement with the values found by calculating the interband emission energy theoretically. We believe that our investigations can stimulate further research in device applications of CdS based materials in future.

References

[1] Yamaguchi T, Yamamoto Y, Tanaka T, Demizu Y and Yoshida A 1996 *Thin Solid Films* **375** 281

[2] Yamaguchi T, Matsufusa J and Yoshida A 1992 *Jpn. J. Appl. Phys.* **3** L703

[3] Walter T, Ruckh M, Velthaus K O and Schock H W 1992 *Proceedings of the 11th EC Photovoltaic Solar Energy Conference* p. 124

[4] Manaselyan A and Chakraborty T 2010 *Nanotechnology* **21** 355401

[5] Karar N, Singh F and Mehta B R 2004 *J. Appl. Phys.* **95** 656

[6] Haranath D, Bhalla N, Chandra H, Rashmi, Kar M and Kishore R 2004 *J. Appl. Phys.* **96** 6700

[7] Jung D R, Son D, Kim J, Kim C and Park B 2008 *Appl. Phys. Lett.* **93** 163118

[8] Wang W, Huang F, Xia Y and Wang A 2008 *Journal of Luminescence* **128** 610

[9] Xiao Q and Xiao C 2008 *Appl. Surf. Sci.* **254** 6432

[10] Sethi R, Kumar L, Sharma P K and Pandey A C 2010 *Nanoscale Research Letters* **5** 96

[11] Kim S Y, Kim D S, Ahn B T and Im H B 1993 *J. Mater. Sci. Mater. Electron.* **4** 178

[12] B J Wu B J, Cheng H, Guha S, Hasse M A, De Puydt J M, Meis-Haugen G and Qiu J 1993 *Appl. Phys. Lett.* **63** 2935

[13] Bailey R E and Nie S J 2003 *J. Am. Chem. Soc.* **125** 7100

[14] Zhong X, Feng Y, Knoll W and Han M 2003 *J. Am. Chem. Soc.* **125** 13559

[15] Cizeron J and Pileni M P 1995 *J. Phys. Chem.* **99** 17410

[16] Lee J H, Song W C, Yi J S, Yang K J, Han W D, Hwang J 2003 *Thin Solid Films* **431** 349

[17] Wu B J, Cheng H, Guha S, Haase M A, Depuydt J and Meishaugen Q G 1993 *J. Appl. Phys. Lett.* **63** 2935

[18] Sharma P K, Dutta R K, Kumar M, Singh P K and Pandey A C 2009 *J. Luminescence* **129** 605

[19] Keshari A K and Pandey A C 2009 *J. Appl. Phys.* **10** 5064315

[20] Yoshikawa A, Okamoto T, Yasuda H, Yamaga S and Kasai H 1990 *J. Crystal Growth* **101** 86

[21] Yamaguchi K and Sato S 1984 *Jpn. J. Appl. Phys.* **23** 126

[22] Karasawa T, Ahkawa K and Mitsuyum T 1991 *J. Appl. Phys.* **69** 3226

[23] Rossetti R, Hull R, Gibson J M and Brus L E 1985 *J. Chem. Phys.* **82** 552

[24] Karar N, Jayaswal M, Halder S K and Chandra H 2007 *J. Alloys Compd.* **436** 61

[25] Padam G K, Malhotra G L and Rao S U M 1988 *J. Appl. Phys.* **63** 770

[26] Hwak H L 1983 *J. Phys.* D: *Appl. Phys.* **D16** 2367

[27] Eason R 2007 *Pulsed Laser Deposition of Thin Films* (New Jersey: Wiley)

[28] Bir G L and Pikus E 1974 *Symmetry and Strain-Induced Effects in Semiconductors* (New York: Wiley)

[29] Singh J 1996 *Optoelectronics: An Introduction to Materials and Devices* (New Delhi: Tata McGraw Hill)

[30] Chuang S L 1995 *Physics of Optoelectronic Devices* (New York: John Wiley & Sons)

[31] Shi J J and Gan Z Z 2003 *J. Appl. Phys.* **94** 407

[32] Park K C and Im H B 1998 *Journal Electrochemical Society Solid State Science and Technology* **135** 793

[33] Xing C, Zhang Y, Yan W, *et al.* 2006 *Science International Journal of Hydrop Energy* **31** 2018

[34] Padam G K, Malhotra G L and Rao S U M 1988 *J. Appl. Phys.* **63** 770

[35] Jana S, Maity R, Das S, Mitra M K and Chattopadhyay K K 2007 *Sci. Phys.* E **39** 109

[36] Padam G K, Rao S K M and Malhotra G L 1998 *Proc. 27th IEEE Photovoltaic Specialists Conference* (New York: IEEE) **II** P. 1591

[37] Rameshwar N. Bhargava, D. Haranath and Adosh Mehta 2008 *J. Korean Phys. Soc.* **53** 2847

[38] Koga T, Nitta J, Takayanagi H and Datta S 2002 *Phys. Rev. Lett.* **88** 126601

[39] Vladimir A, Fonoberov and Alexander A Balandin 2004 *Appl. Phys. Lett.* **85** 5971

[40] Mohanta D, Narayanan S S, Pal S K and Raychaudhuri A K 2009 *J. Experimental Nanoscience* **4** 177

[41] Wang X, Qu L, Zhang J, Peng X and Xiao M 2003 *Nano Lett.* **3** 1103

[42] Anil T V, Menon C S, Jayachandran K P and Shree Krishna K K 2006 *J. Mater. Sci.* **41** 8013

[43] Srinivasa Rao B and Paul H S 1969 *Applied Scientific Research* **20** 251

[44] Ben Afia S and Belmabrouk H 2008 *Thin Solid Films* **516** 1608